ORIGINAL ARTICLE

Hydrogel Production Platform with Dynamic Movement Using Photo-Crosslinkable/Temperature Reversible Chitosan Polymer and Stereolithography 4D Printing Technology

Jeong Wook Seo[1] · Su Ryon Shin[2] · Yeon Joo Park[3] · Hojae Bae[1]

Abstract

BACKGROUND: Three-dimensional (3D) printing using hydrogel has made great strides when it comes to mimicking 3D artificial tissue in the medical field. However, most structures do not mimic the dynamic movement of the tissues. Without imitating dynamic movements, there are limitations on the extent to which the proper implementation of the tissue's own functions can be achieved.

METHOD: In this study, we intend to present an approach to solving this problem using hydroxybutyl methacrylated chitosan (HBC-MA), a photo-crosslinkable/temperature reversible chitosan polymer. In addition, stereolithography-3D (SLA-3D) printing technology was used, which is more likely to mimic the complex microstructure. As a control, a 3D structure made with pristine poly(ethylene glycol) dimethacrylate (PEG-DMA) was created, and a 4D structure was prepared by adding HBC-MA to poly(ethylene glycol) dimethacrylate (PEG-DMAP) resin.

RESULTS: HBC-MA caused the expansion of water into the polymer matrix at low temperature, and the 4D structure resulted in expansion of the polymer volume, generating dynamic movement due to the expansion of water. Conversely, as the temperature rose, deswelling occurred, followed by a decrease in the volume, showing a shape memory property of returning to the existing structure. Morphological, swelling, and mechanical analysis further confirmed the principle of dynamic movement. In addition, parameters were provided through calculation of the bending ratio angle (θ).

CONCLUSION: Through this, it is suggested that HBC-MA can be applied as a core polymer for SLA-4D printing, and has high potential for realizing the dynamic movement of tissue.

Keywords Hydroxybutyl chitosan · SLA-3D printing · 4D printing · Shape memory property (SMP)

✉ Hojae Bae
hojaebae@konkuk.ac.kr

1 Department of Stem Cell and Regenerative Biotechnology, KU Convergence Science and Technology Institute, Konkuk University, Hwayang-dong, Gwangjin-gu, Seoul 05029, Republic of Korea

2 Division of Engineering in Medicine, Department of Medicine, Brigham and Women's Hospital, Harvard Medical School, Cambridge, MA 02139, USA

3 Department Bioindustrial Technologies, College of Animal Bioscience and Technology, Konkuk University, Seoul 05029, Republic of Korea

1 Introduction

Over the last decade, three-dimensional (3D) printing has shown great potential for the development of 3D artificial tissue mimics using nano/micro hydrogel structures. Most of these studies have focused on the application of 3D printed structures in the medical field; for example, plastic surgery applications through morphological imitation of organs made of soft tissues such as ears [1, 2] or nose [3, 4]. However, such structures do not mimic the dynamic movements of the organ. Fabricated organs that are built without imitating dynamic responses are limited in terms of their own function implementation. For instance, the response of the hypothalamus to a rise in body temperature

is controlled by the expansion of blood vessels, resulting in increased sweat secretion through the glands of skin tissue [5, 6]. Peristaltic movement of the digestive system controlled by nerve relaxation and contraction of muscles are also representative examples [7, 8]. In addition, morphological changes in tissue structure have a profound effect on natural tissue regeneration and repair [9]. Thus, conventional 3D structures with static properties are limited in their use. To this end, a concept of time is added to a conventional 3D structure, and a stimulus-responsive biocompatible material that can incorporate a shape conversion function to implement four-dimensional (4D) printing capable of dynamic structural change and response to the environment is required.

4D printing is defined as a 3D printed structure capable of showing recognizable morphological deformation over time. Morphological deformation is caused by changes in the physical properties (e.g. swelling) or mechanical strength of the active components of the structure, such as swelling ratio, expansion, and contraction, etc. [10]. The shape memory property (SMP), which reverts to the original structure after transformation, also enables reversible shape transformation.

Lithography-based printing technologies, such as stereolithography (SLA) or digital light processing (DLP), have shown great potential to further mimic the complex structure and microenvironment of biological tissues by utilizing photocrosslinkable resins [11, 12]. It is a platform technology that can achieve the goal of tissue engineering, such as the production of artificial organs and artificial meat. However, compared to other 3D printing methods, there are fewer cases of hydrogel printing through the stereolithography-3D (SLA-3D) printer, and cases of implementing 4D printing are also very rare. Therefore, this study will introduce 4D printing through an SLA 3D-printing method (Fig. 1A). In SLA-printing, a polymer-based resin satisfying several conditions is required to successfully accomplish 4D printing. Since lamination is based on photopolymerization by a laser, SLA-printing requires a polymer that can be photo-crosslinked. In the case of 4D printing, changes in the shape, properties, and functions of the printed structure should be induced according to the stimulus [13–15]. Finally, the organ's movement should have SMP, because it is a transformation that reverts to its original form by reversible change. Once these three requirements are realized, 4D properties can be assigned to existing 3D structures.

In this study, we hypothesized that hydroxybutyl methacrylated chitosan (HBC-MA), a dual-crosslinkable biomaterial, meets the above criteria. HBC-MA is a novel material developed in our previous study, a photocrosslinkable temperature-reversible chitosan polymer, which reacts sensitively to temperature changes

(Unpublished data). At low temperatures (T < 20 °C), swelling of the water within the polymer matrix takes place. On the other hand, when the temperature rises (T > 30 °C), a temperature-tunable pore is formed, resulting in deswelling. Taking advantage of these temperature-responsive features, swelling was generated in the 3D structure at low temperature, resulting in the shape change through expansion of the volume. At high temperatures, additional micropores were generated within the polymer matrix, followed by water release. Through this study, 4D structures with HBC-MA could be realized through SMP such that the volume of the polymer that is expanded by swelling of water contracts again and returns to the original shape. Through this, we suggest that HBC-MA can be applied as a core polymer for SLA-4D printing.

2 Materials and methods

2.1 Materials

Chitosan (low molecular weight), methacrylic anhydride (MA, 94.0%), 1,2-epoxybutane, eosin Y (dye content ∼ 99%), triethanolamine (TEA, ≥ 99.0%), 1-vinyl-2-pyrrolidinone (NVP, contains sodium hydroxide as an inhibitor, ≥ 99.0%), and phenylbis (2,4,6-trimethylbenzoyl) phosphine oxide (BAPOs) were purchased from Sigma-Aldrich (St. Louis, MO, USA). Poly(ethylene glycol) dimethacrylate (PEG-DMA, MW 1,000) was purchased from Polysciences (Warrington, PA, USA). Cellulose nanofibrils (CNF, 3 wt %) were provided by Celluloselab (Fredericton, New Brunswick, Canada). Phosphate-buffered saline (pH 7.4, PBS) was purchased from WelGene (Daegu, Gyeongbuk, Korea). All other chemical agents used in this paper were analytical grade.

2.2 Preparation of hydroxybutyl methacrylated chitosan (HBC-MA)

Two substituents should be substituted for pure chitosan to produce HBC-MA for SLA-4D printing. Based on previous experiments, 10 g of chitosan was completely dissolved in 600 ml of 0.1 M Acetic acid, after which pH was adjusted to 6 using 5 M NaOH, followed by the addition of 200 ml of 1,2-epoxybutane (99%). The mixture was then reacted at 60 °C for 24 h. After the reaction was complete, washing was performed using a centrifuge to remove any remaining 1,2-epoxybutane. Finally, hydroxybutyl chitosan (HBC) solution was lyophilized for 4 days [16]. To make HBC-MA, 10 g of the recovered HBC was dissolved in 600 ml of distilled water overnight followed by the addition of 15% (v/v) methacrylic anhydride (94%) and left for 4 h (pH 7). The mixture was dialyzed against distilled water
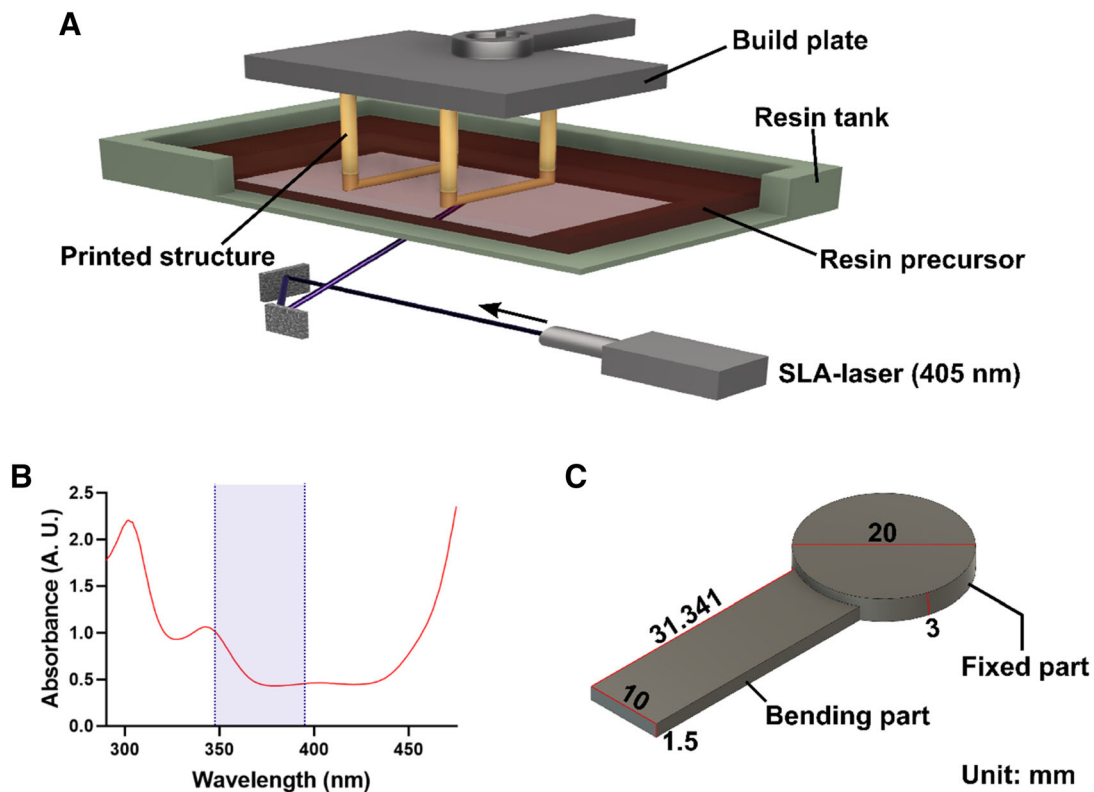
Fig. 1 A Schematic describing the SLA-3D printing process for structure fabrication using resin precursors. The SLA-laser, which is beamed under the resin tank, causes the resin to build up under the build plate during photo-crosslinking. **B** Spectrum of light absorbance for 4D resin solution. The purple region is the expected laser output wavelength region of Form 2. **C** 3D model designed for 4D hydrogel construct. The 4D printing model consists of a fixed part and a bending part. All units are in mm

for 1 week using dialysis tubing (12–14 kDa cut-off) to remove residual methacrylic anhydride, and finally the purified HBC-MA polymer was lyophilized [17].

2.3 Preparation of 4D resin formulation

We prepared 4D resins for SLA printing by compounding the HBC-MA with a PEG-DMA, CNF, and photoinitiator. For 4D printing characteristics, the resins were prepared by combining 2% (w/v) HBC-MA, 15% (w/v) PEG-DMA, 0.5% (w/v) CNF, and the photoinitiatior. CNF is physically confined in the photocrosslinked hydrogel to assist in the directionality of volume expansion and swelling rate [18]. Photoinitiator was prepared using 0.1 mM Eosin Y, 0.75% (v/v) TEA, 1% (v/v) NVP, and 0.03% (w/v) BAPOs. Eosin Y, TEA, and NVP were prepared according to the previously reported composition with minimal cytotoxicity [19]. The BAPOs was also added to increase the responsiveness to UV-wavelength lasers (Fig. 1B). The control resin formulation (Table 1), which is the same as the 4D resin formulation but excludes HBC-MA, was also prepared as a control.

2.4 SLA-3D printing setting

Prior to printing, air bubbles generated within the resin solution during the mixing process were removed, and 150–200 ml of resin was poured into the resin tank. Then, Form2 (Formlabs, Somerville, MA, USA), a commercial SLA-3D printer, was used for all printing processes, which were performed at room temperature with a layer thickness of 100 μm. The fabricated control and 4D structures were carefully removed from the build plate once the printing was complete.

2.5 Preparation of 3D models

For the preparation of 3D models, a measurement model and a 4D printing model were designed separately. The measurement model was designed in a form that allows accurate analysis to measure mechanical properties and mass swelling ratios. The measurement model was designed as a flat cylindrical model with a diameter of 20 mm and a height of 4 mm (no image). The 4D printing model was made of a combination of fixed and bending parts (Fig. 1C). The fixed part is a cylindrical model with a diameter of 20 mm and a height of 3 mm. The bending part

Table 1 Control and 4D resin formulation used for 4D SLA-printing

Type	HBC-MA[a] (%, w/v)	PEG-DMA[b] (%, w/v)	CNF[c] (%, w/v)	Photoinitiator			
				Eosin Y (mM)	TEA[d] (%, v/v)	NVP[e] (%, v/v)	BAPOs[f] (%, w/v)
Control resin	–	15	0.5	0.1	0.75	0.4	0.03
4D resin	2	15	0.5	0.1	0.75	0.4	0.03

[a]Hydroxybutyl methacrylated chitosan

[b]Poly(ethylene glycol) dimethacrylate

[c]Cellulose nanofibrils

[d]Triethanolamine

[e]1-Vinyl-2-pyrrolidinone

[f]Phenylbis (2, 4, 6-trimethylbenzoyl) phosphine oxide

is an elongated model with a width of 31.341 mm, a length of 10 mm, and a height of 1.5 mm. All models were designed using Fusion 360 software (Autodesk, Mill Valley, CA, USA). Prior to printing, preforming software (Formlabs) support settings were configured. Supporting setting parameters for all resins were: Density of 1.00; Touch size of 2.20 mm; Slope spacing of 1.00; Z-compression connection of 0.75 mm; Early layer merge of 0.45 mm.

2.6 Changes in properties of printed structures with temperature

2.6.1 Morphological studies

Scanning electron microscopy (SEM) was performed on control and 4D hydrogel samples to obtain information on the pore structure of hydrogels. Two types of structures (control and 4D structures) were prepared with three temperature groups (10, RT, and 37 °C) to confirm the difference in pore structure. All samples were stored in PBS at each temperature immediately after printing, and were lyophilized to maintain the pore structure and ensure no collapse. After lyophilization, samples were cross-sectioned at the bending position and then secured on a stub via carbon tapes coated with platinum. Cross-sectional morphologies were imaged with an SU-8010 scanning electron microscope (Hitachi, Tokyo, Japan).

2.6.2 Swelling properties

To measure the difference in water content over temperature, a model design for measurement model (described in 2.5) was printed with two types of resins (control and 4D resin precursors). Two types of structures (control and 4D structures) were produced to confirm the difference in moisture content. All samples were stored in PBS at three different temperatures (10, RT, and 37 °C) immediately

after printing and measurements were taken after 24 h. After the measurement of the swollen weight (S_w), samples were immediately frozen in liquid nitrogen to minimize the effect of temperature changes. After lyophilization, the dry weight (D_w) was measured. Finally, swelling ratio (%) was calculated as follows:

$$\text{Swelling ratio } = \frac{S_w}{D_w},$$

2.7 Mechanical properties

To test the mechanical properties, control and 4D resin precursors were printed in a measurement model (described in 2.5). A CT3 Texture analyzer (Brookfield; Toronto, ON, Canada) with a 4,500 g load cell in compression mode was used to measure the compressive strength of printed structures. A probe 12.7 mm in diameter was used to compress with a trigger load of 0.05 N at a test speed of 0.05 mm/s. The compressive modulus was determined as the slope of the linear region corresponding to 5–15% strain [20]. Four-dimensional (4D) structures were prepared in three temperature groups (10, RT, and 37 °C) to confirm the difference in strength. All samples were stored in PBS at their own temperature immediately after printing and measured after 24 h.

2.8 Calculation of bending ratio of 4D structures

The bending ratio was calculated to determine the dynamic characteristics of the 4D structure with the change of ambient temperature. First, a 4D printing model (described in 2.5) was printed with 4D resin precursor. The bending part of the printed 4D structure was bent while swelling at 10 °C. Then, it was deswelled under heating (37 °C) and unbent again. The bending part was assumed to be bent upwards with volume expansion based on the swelling of the water. Therefore, we approached the method of calculating the bending ratio angle (θ) by measuring the

expanding base side (a) and the height (b) (Fig. 4A). The images were taken at 10 s intervals. Bending ratio angle (θ) was calculated as follows:

$$\text{bending ratio angle } (\theta) = \tan^{-1}\left(\frac{b}{a}\right)$$

3 Results and discussion

3.1 SLA-3D printing process and resin component

The purpose of this study is to produce 4D scaffolds with dynamic characteristics by adding HBC-MA to the existing 3D resins with static characteristics. The SLA-laser (405 nm) emitted from the bottom of the machine reaches the resin precursor in the resin tank through the reflector. The methacrylate portion of PEG-DMA and HBC-MA in the resin precursor crosslinks via photo-initiators. Resin precursor was photopolymerized on the build plate, and hydrogel was formed. Then, when the build plate rises upward, the hydrogel was formed layer by layer and finally the 3D printed structure was fabricated (Fig. 1A). The main photoreaction wavelength range of the photoinitiator of the resin precursor produced in this study was confirmed through a UV–vis spectrometer (Fig. 1B). The laser wavelength ranges of Form2 are displayed in purple. Various sources such as laser wavelength, laser exposure time, and laser intensity output in the flexible V2 mode of the commercial Form2 machine have not been published. However, in the flexible V2 mode of Form2, the control and 4D resins produced in this study were capable of printing 3D constructs successfully. Development and characterization of dual-crosslinkable HBC-MA have been described in our previous work (Unpublished data). Photo-crosslinked HBC-MA hydrogels undergo additional thermal-crosslinking due to hydrophobic interaction when the ambient temperature rises. The thermal-crosslinking process not only forms additional pores within the hydrogel but also involves deswelling of the water [21, 22]. On the other hand, when the ambient temperature drops, the hydrophobic interactions are released, increasing the rate of water expansion as the hydrophilic chains are revealed [22, 23]. Based on this characteristic of HBC-MA, it was hypothesized that a 4D printing structure with reversible temperature sensitivity could be produced. The composition of the 4D resin produced was optimized to achieve this purpose. Of the many polymers capable of forming a 3D scaffold, PEG-DMA was selected as a representative polymer [24, 25]. In conclusion, the 4D resin precursor was prepared by adding only HBC-MA to the composition of the control resin precursor composed of PEG-DMA (Table 1).

3.2 3D modeling for 4D structure

To observe and analyze the dynamic motion of 4D printing underwater, a standard 4D printing model was required. The designed 3D model was divided into a fixed part and a bending part. The fixed part was made in the shape of a circle so as not to have any movement upon expansion. The fixed part, which has no directional guidance in the only direction, did not express dramatic dynamic movement. This prevented unexpected movements such as flipping or floating. The bending part is designed to have an elongated shape in order to facilitate bending upon expansion in a certain direction. The proposed design enabled facile visual observation of the dynamic movements and the analysis (Fig. 1C).

## 3.3 Property change with temperature of printed structure

3.3.1 Morphological analysis

To demonstrate the use of HBC-MA as a potential material for introducing 4D systems into existing 3D structures, we examined the change in pore characteristics with change in temperature. Unlike the control structure, the 4D structure mixed with HBC-MA realized dynamic bending and unbending with temperature (Fig. 2A). In the control structure without HBC-MA, formation of pores or cracks with temperature change was not observed (Supplementary Fig. 1). However, in the 4D structure mixed with HBC-MA, micrometer-sized pores were observed immediately after printing (Fig. 2B). After the temperature was lowered (10 °C), elongated cracks were observed in the SEM images (Fig. 2C). According to the pore formation characteristics of HBC-MA, it was confirmed that many cracks occurred due to bending and swelling. After increasing the temperature (37 °C), it was confirmed that a number of pores were additionally generated by thermal-crosslinking of HBC-MA (Fig. 2D). From the image, it was confirmed that unlike the control structure, the 4D printing structure has a characteristic of reversible pore structure formation depending on the temperature.

3.3.2 Swelling analysis

A mass swelling test was conducted to understand the principle of shape deformation of a 4D structure. The 4D structure loaded with HBC-MA showed dynamic swelling characteristics with temperature. For the group stored at 37 °C for 24 h after printing with the 4D resin precursor, a
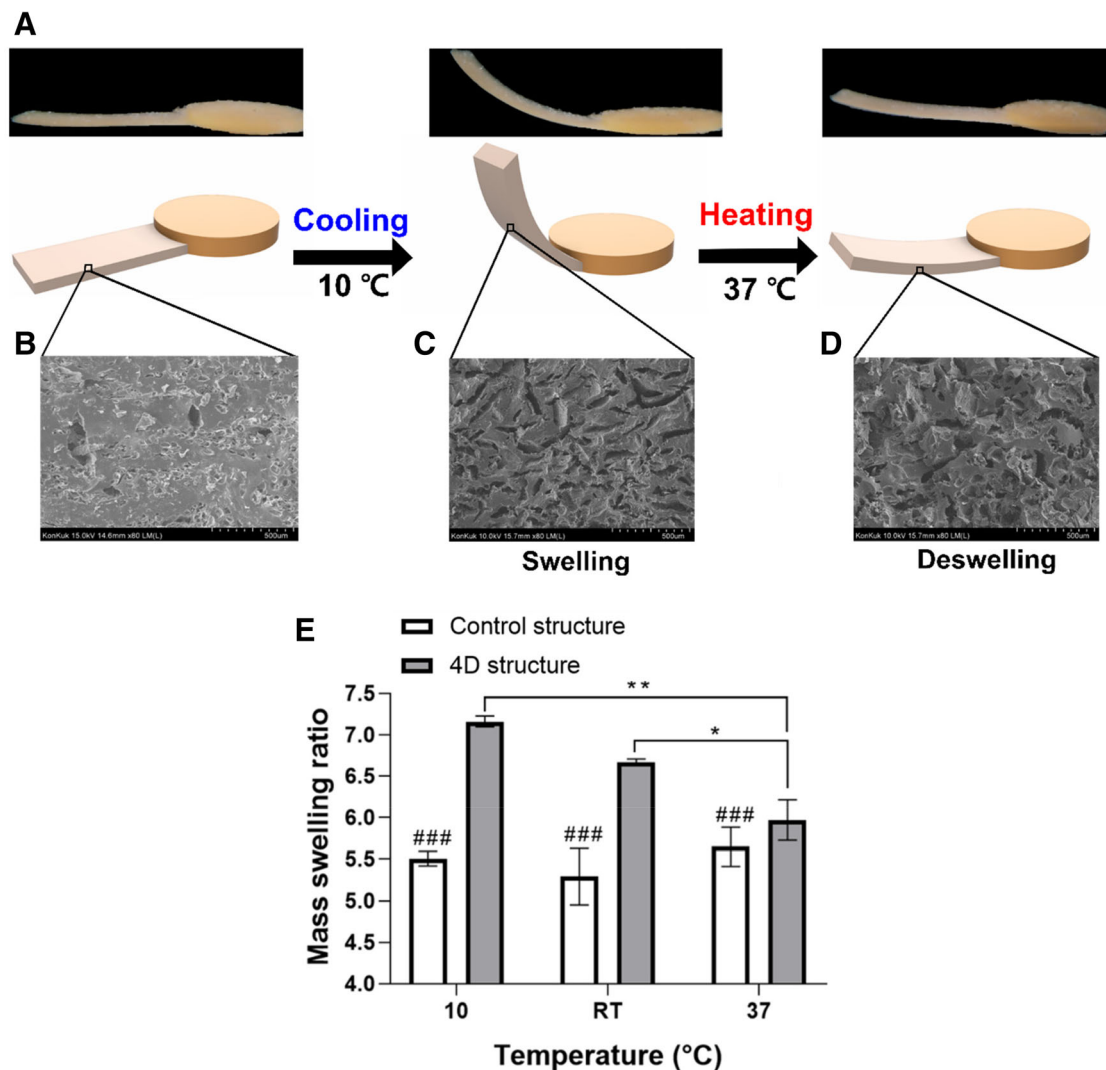
Fig. 2 A Schematic describing the entire process of reversible dynamic movement of 4D printing. The 4D structure produced by the 4D printing modeling design showed bending movements upon cooling and unbending movements upon heating. **B** Pore structure of the printed 4D structure. Small pores formed by HBC-MA are observed between the pore-free walls made of photopolymerized PEG-MA. **C** Pore structure after bending. Cracks from bending during swelling were observed. **D** Pore structure after unbending. At 37 °C, thermal-crosslinked pores with deswelling were observed. **E** Equilibrium swelling characteristics of control vs 4D printing structure. The 4D structure showed different swelling ratios with temperature. There was no statistically significant difference with temperature in the control group. *$p < 0.05$, **$p < 0.01$ between the indicated group; ###$p < 0.001$ versus 10 °C group of 4D structure. Data are shown in mean ± SD, n = 3

swelling ratio of 5.97 ± 0.24 was measured. In comparison, the group stored at RT measured 6.67 ± 0.04 (*$p < 0.05$) and the group stored at 10 °C after printing was 7.16 ± 0.07 (**$p < 0.01$), respectively. As expected, the cooling (10 °C) group, where 4D printing bending occurred, was found to have the highest swelling ratio. On the other hand, the heating (37 °C) group exhibited an unbending phenomena, and it was confirmed by analysis that water was discharged due to deswelling at the lowest swelling ratio. Within the control structure group, there was no statistically significant difference in the swelling ratio according to change in temperature. However, all the groups in the control structure samples showed statistically significant differences from the cooling (10 °C) group of the 4D structure (###$p < 0.001$). These results confirm that the volume difference due to swelling and deswelling according to the change in temperature resulted in shape deformation, enabling a 4D characteristic.

3.3.3 Mechanical analysis

The mechanical performance of printed structures was characterized to evaluate their potential for use in applications. The compressive modulus was measured to be

219.57 ± 128.93 kPa in the cooling (10 °C) group in the 4D structure type. The RT and heating (37 °C) groups were measured at 369.31 ± 120.75 kPa and 543.91 ± 69.38 kPa, respectively (Fig. 3A). As shown in the representative stress–strain curves of a 4D structure containing HBC-MA, the stiffness increased at all strain levels with respect to temperature rise under all conditions (Fig. 3B). It has been reported that the expansion ratio of volume and mechanical properties were inversely proportional [26]. The results of this study also confirmed that the results of mechanical analysis and the results of swelling ratio are inversely proportional to each other. The difference in mechanical properties with temperature is determined by HBC-MA. Thermal-crosslinking of HBC-MA due to the rise in temperature would not only form additional pores, but also would reduce the moisture content, resulting in a denser network. On the other hand, the decrease in temperature caused swelling in the HBC-MA polymers and lowered the mechanical strength due to the loose network configuration and decreased density caused by the expanded volume as a result of the increased water content. The data showed that the temperature sensitivity imparted by HBC-MA closely influenced the mechanical strength of the 4D structure.

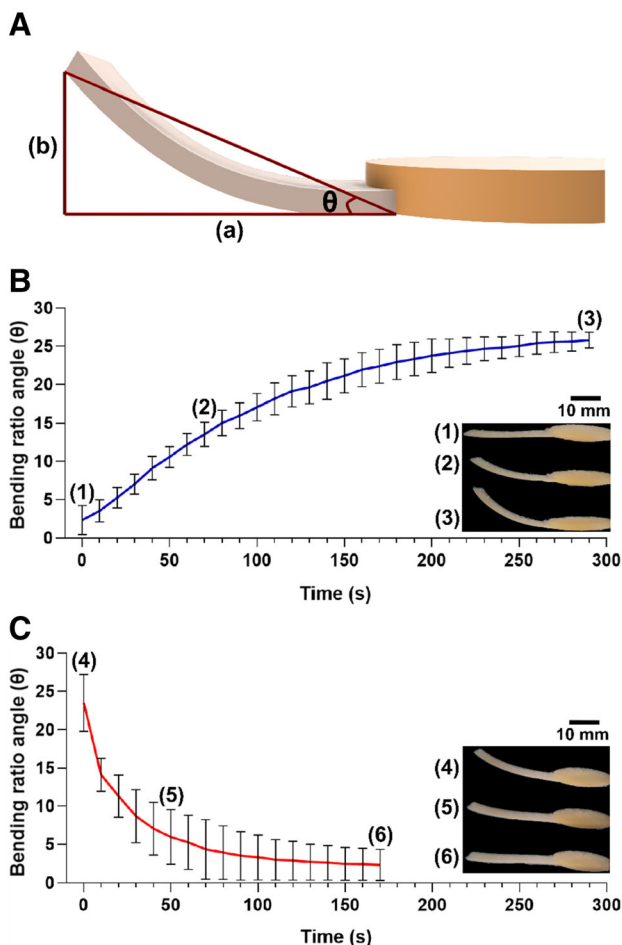### 3.4 Bending ratio of 4D structure evaluation

Dynamic movement according to the temperature change of a 4D resin structure containing HBC-MA is expressed by bending and unbending. Therefore, the 4D printing capability of the HBC-MA can be confirmed and parameters can be organized by calculating the ratio angle (θ) of bending and unbending. The bending ratio calculation method used in this study expresses the bending curvature of 4D printing as a relative ratio. The 4D structure with HBC-MA was able to provide parameters by calculating

the bending ratio angle through optically measuring bending with temperature at intervals of 10 s. Under cooling conditions (10 °C), the 4D structure was expressed by a bending shape deformation through swelling of water. The bending ratio angle (θ) gradually increased while the length of the base side (a) decreased and the length of the height (b) increased. The bending ratio angles at the lowest point (1), midpoint (2), and the highest point (3) were 2.35 ± 1.91, 13.55 ± 1.58, and $25.82 \pm 1.03°$, respectively (Fig. 4B and Supplementary movie 1). When the bent 4D structure was heated (37 °C), HBC-MA caused a volume shrinkage through deswelling as a stimulus–response to temperature. Volumetric contractions are expressed as unbending back to its original form. As the length of the base side (a) increased and the height (b) decreased, the bending ratio angle (θ) decreased rapidly. The shape deformation rate is faster during heating than during cooling. Under heating conditions, the bending ratio angles at the highest point (4), middle point (5), and the lowest point (6) were 23.51 ± 3.71, 5.96 ± 3.57, and $2.31 \pm 2.03°$, respectively (Fig. 4C and Supplementary movie 2).

In this study, we demonstrated the use of HBC-MA for 4D SLA-printing applications, highlighting the unique characteristics that make HBC-MA a potential material for creating dynamic response. The HBC-MA was mixed with a general 3D resin precursor and showed good printability by an SLA-3D printer. It has been also confirmed that printing could be performed with PEG-DMA, a representative SLA-3D printer material. The 4D structure with HBC-MA showed tunable physicochemical properties (e.g., morphology, swelling, and mechanics) according to temperature, and was capable of dynamic movement through volume expansion and contraction. The HBC-MA gave the 4D structure an SMP that reverts to shape deformation through reversible temperature-crosslinking
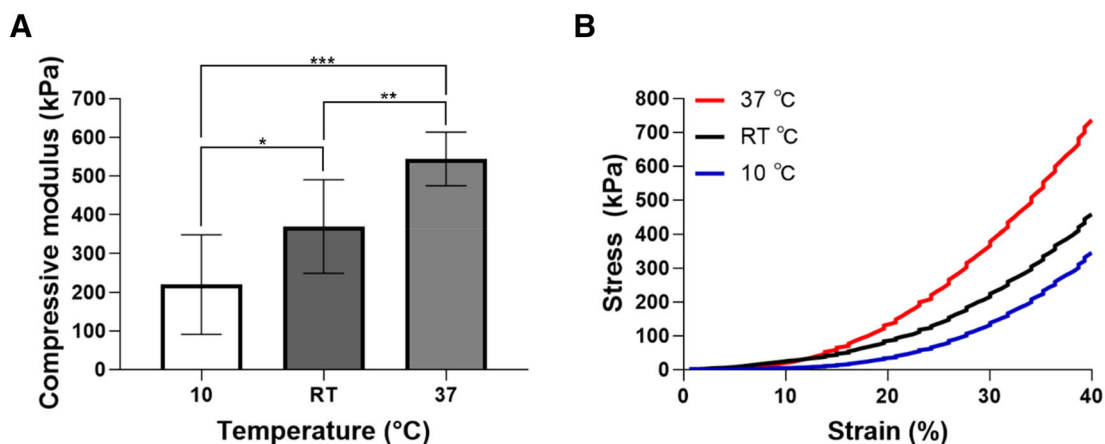
Fig. 3 **A** Compressive modulus of 4D structure at 10, RT, and 37 °C. $*p < 0.05$, $**p < 0.01$, and $***p < 0.001$ between the indicated group. Data are shown in mean $\pm$ SD, n = 10. **B** A representative stress–strain curve of 4D structure at 10, RT, and 37 °C

A

B

C

Fig. 4 A Schematic for the calculation of the bending ratio angle (θ) of 4D structures. The bending ratio angle (θ) was calculated from the measured values of the base side (a) and height (b) of the triangle. **B** Bending ratio angle (θ) graph of 4D structures under cooling (10 °C) condition. **C** Bending ratio angle (θ) graph of 4D structures under heating (37 °C) condition. Photographs of samples are shown as numbered

properties. In conclusion, HBC-MA can be regarded as a potential material for tissue engineering and medical applications with 4D printing properties.

Compliance with ethical standards

Conflict of interest The authors declare that they have no financial or commercial conflicts of interest that are directly related to the content of this article.

Ethical statement All the authors declare that there are no ethical issues for humans and animals.

References

1. Morris VB, Nimbalkar S, Younesi M, McClellan P, Akkus O. Mechanical properties, cytocompatibility and manufacturability of chitosan: PEGDA hybrid-gel scaffolds by stereolithography. Ann Biomed Eng. 2017;45:286–96.
2. Jung BK, Kim JY, Kim YS, Roh TS, Seo A, Park KH, et al. Ideal scaffold design for total ear reconstruction using a three-dimensional printing technique. J Biomed Mater Res B Appl Biomater. 2019;107:1295–303.
3. Goyanes A, Det-Amornrat U, Wang J, Basit AW, Gaisford S. 3D scanning and 3D printing as innovative technologies for fabricating personalized topical drug delivery systems. J Control Release. 2016;234:41–8.
4. Nuseir A, Hatamleh MM, Alnazzawi A, Al-Rabab'ah M, Kamel B, Jaradat E. Direct 3D printing of flexible nasal prosthesis: optimized digital workflow from scan to fit. J Prosthodont. 2019;28:10–4.
5. Fortney SM, Nadel ER, Wenger CB, Bove JR. Effect of blood volume on sweating rate and body fluids in exercising humans. J Appl Physiol Respir Environ Exerc Physiol. 1981;51:1594–600.
6. Wendt D, van Loon LJC, Lichtenbelt WDM. Thermoregulation during exercise in the heat. Sports Med. 2007;37:669–82.
7. Costa M, Furness JB. The peristaltic reflex: an analysis of the nerve pathways and their pharmacology. Naunyn Schmiedebergs Arch Pharmacol. 1976;294:47–60.
8. Kunze WA, Furness JB. The enteric nervous system and regulation of intestinal motility. Annu Rev Physiol. 1999;61:117–42.
9. Xiao Y, Ahadian S, Radisic M. Biochemical and biophysical cues in matrix design for chronic and diabetic wound treatment. Tissue Eng Part B Rev. 2016;23:9–26.
10. Momeni F, Hassani.N SMM, Liu X, Ni J. A review of 4D printing. Mater Des. 2017;122:42–79.
11. Wu GH, Hsu SH. Review: polymeric-based 3D printing for tissue engineering. J Med Biol Eng. 2015;35:285–92.
12. Ma X, Qu X, Zhu W, Li YS, Yuan S, Zhang H, et al. Deterministically patterned biomimetic human iPSC-derived hepatic model via rapid 3D bioprinting. Proc Natl Acad Sci U S A. 2016;113:2206–11.
13. Ge Q, Dunn CK, Qi HJ, Dunn ML. Active origami by 4D printing. Smart Mater Struct. 2014;23:094007.
14. Kuksenok O, Balazs AC. Stimuli-responsive behavior of composites integrating thermo-responsive gels with photo-responsive fibers. Mater Horiz. 2016;3:53–62.
15. Bakarich SE, Gorkin R 3rd, in het Panhuis M, Spinks GM. 4D printing with mechanically robust, thermally actuating hydrogels. Macromol Rapid Commun. 2015;36:1211–7.
16. Tsukamoto Y, Akagi T, Shima F, Akashi M. Fabrication of orientation-controlled 3D tissues using a layer-by-layer technique and 3D printed a thermoresponsive gel frame. Tissue Eng Part C Methods. 2017;23:357–66.
17. Yoon HJ, Shin SR, Cha JM, Lee SH, Kim JH, Do JT, et al. Cold water fish gelatin methacryloyl hydrogel for tissue engineering application. PLoS One. 2016;11:e0163902.
18. Gladman AS, Matsumoto EA, Nuzzo RG, Mahadevan L, Lewis JA. Biomimetic 4D printing. Nat Mater. 2016;15:413–8.
19. Shih H, Fraser AK, Lin CC. Interfacial thiol-ene photoclick reactions for forming multilayer hydrogels. ACS Appl Mater Interfaces. 2013;5:1673–80.
20. Nichol JW, Koshy ST, Bae H, Hwang CM, Yamanlar S, Khademhosseini A. Cell-laden microengineered gelatin methacrylate hydrogels. Biomaterials. 2010;31:5536–44.
21. Zhang XZ, Chu CC. Preparation of thermosensitive PNIPAAm hydrogels with superfast response. Chem Commun (Camb). 2004;3:350–1.

22. Zhang XZ, Xu XD, Cheng SX, Zhuo RX. Strategies to improve the response rate of thermosensitive PNIPAAm hydrogels. Soft Matter. 2008;4:385–91.

23. Yuan M, Bi B, Huang J, Zhuo R, Jiang X. Thermosensitive and photocrosslinkable hydroxypropyl chitin-based hydrogels for biomedical applications. Carbohydr Polym. 2018;192:10–8.

24. Do AV, Worthington KS, Tucker BA, Salem AK. Controlled drug delivery from 3D printed two-photon polymerized poly(-ethylene glycol) dimethacrylate devices. Int J Pharm. 2018;552:217–24.

25. Kadry H, Wadnap S, Xu C, Ahsan F. Digital light processing (DLP) 3D-printing technology and photoreactive polymers in fabrication of modified-release tablets. Eur J Pharm Sci. 2019;135:60–7.

26. Naficy S, Brown HR, Razal JM, Spinks GM, Whitten PG. Progress toward robust polymer hydrogels. Aust J Chem. 2011;64:1007–25.